

# Stable Aqueous Dispersions of Glycopeptide-Grafted Selectably Functionalized Magnetic Nanoparticles\*\*

Tushar Borase, Tsedev Ninjbadgar, Antonios Kapetanakis, Sandra Roche, Robert O'Connor, Christian Kerskens, Andreas Heise,\* and Dermot F. Brougham\*

Bionanomaterials have received increasing attention over the last decade, owing to their potential to advance medical science by providing novel solutions for disease diagnostics and treatment.<sup>[1]</sup> However, bionanomaterial engineering imposes considerable challenges, as significant design criteria and properties, which are dictated by the specific application, must be met. MRI-trackable magnetic nanoparticles (MNPs) and their assemblies, which are capable of targeting specific cell types, such as cancer cells, for image-guided treatment are increasingly being investigated.<sup>[2]</sup> The typical design criteria for MNPs are biomedical in nature, including cellular selectivity (biorecognition), extended blood circulation times and biocompatibility, there are also practical considerations such as processability and scalability. Additional MRI-specific criteria include colloidal stability and high image contrast. The efficacy of an MNP suspension for generating contrast by enhancing, or suppressing, a local MRI signal is quantified by the spin–lattice ( $r_1$ ) and spin–spin ( $r_2$ ) relaxivities, respectively. These are the water relaxation enhancement per millimolar concentration of iron. For  $T_1$ -weighting applications (localized signal enhancement),  $r_1$  must be high, and  $r_2$  and the  $r_2/r_1$  ratio must be low. Particle aggregation increases the  $r_2$  value, so  $T_1$ -weighting can only be achieved by ensuring full MNP dispersion and long-term colloidal stability.

Monosaccharides offer colloidal stability through charge and steric interactions along with the possibility of cellular targeting, and so have been used to stabilize MNPs. Recently, MNP clusters have been prepared by encapsulation of alkyl-stabilized MNPs using poly(maleic anhydride-*alt*-1-octadecene) followed by EDC coupling of aminated sugars.<sup>[3]</sup> Detailed analysis of the effect of coating on cellular uptake showed that high grafting density is critical for avoiding non-specific cellular interaction. However, the encapsulation approach resulted in extensive aggregation, as is usually the case, thus limiting the possibility of use in a  $T_1$ -weighting application. Aggregation was exploited in a recent report where clickable monosaccharides were used to stabilize MNP clusters using complex peptide linkers,<sup>[3]</sup> which allowed differentiation of cancer cells by quantitative profiling of carbohydrate binding through changes in  $T_2$  (local signal suppression). In a prominent recent example, a range of phosphonate-functionalized sugars were used to fully disperse MNPs, and the effect of MNP size on the  $T_1$ -weighting and hyperthermic properties in vitro were investigated.<sup>[4]</sup> However, only one sugar per linker was possible, thus limiting the total sugar density.

Hence, there is a need for platform technologies that maximize the surface density of functional monosaccharides while allowing full MNP dispersion. Multifunctional polymers have the potential to address the first issue; there have been two recent reports of a “grafting-onto” approach for MNP modification with glycopolymers. However, dispersion proved not to be possible. In the first example, glycosylated polyacrylate was grafted onto silica-coated iron-oxide MNPs.<sup>[5]</sup> Although cellular uptake of the micron-scale aggregates was confirmed, the magnetic component was quite dilute. In the second example, some improvement in colloidal control was achieved using glucosylated poly(pentafluorostyrene) derivatives to produce suspensions of hydrodynamic size ( $d_{\text{hyd}}$ ) ranging from 100–300 nm.<sup>[6]</sup> However, the polydispersity index (PDI) from dynamic light scattering was quite high ( $> 0.22$ ), which suggests non-uniform particles.

Herein, we describe the novel combination of a polymer “grafting-from” approach with glycosylation by click chemistry for preparing MNPs with a high surface density of monosaccharides. We hypothesized that this would promote dispersibility and, based on the important role of carbohydrates in cell interaction/recognition,<sup>[7]</sup> introduce biorecognition. The polymers are synthetic polypeptides and thus rely on natural degradable building blocks (amino acids). This is the first report of glycopeptide-grafted superparamagnetic  $\text{Fe}_3\text{O}_4$  nanoparticles (GP-MNP), which exhibit excellent water

[\*] T. Borase,<sup>[†]</sup> Dr. T. Ninjbadgar,<sup>[†]</sup> A. Kapetanakis, Dr. A. Heise, Dr. D. F. Brougham  
School of Chemical Sciences, Dublin City University  
Glasnevin, Dublin 9 (Ireland)  
E-mail: andreas.heise@dcu.ie  
dermot.brougham@dcu.ie

Dr. S. Roche, Dr. R. O'Connor, Dr. D. F. Brougham  
National Institute for Cellular Biotechnology, Dublin City University  
Glasnevin, Dublin 9 (Ireland)

Dr. C. Kerskens  
Institute of Neuroscience, University of Dublin  
Trinity College, Dublin 2 (Ireland)

[†] These authors contributed equally to this work.

[\*\*] T.N., C.K., and D.B. acknowledge support from Enterprise Ireland (TD20080135). S.R. acknowledges the DCU Targeted Research Initiative Fund (TRIF). A.H. and T.B. acknowledge Science Foundation Ireland for a Principle Investigator Award (07/IN1/B1792). A.K. acknowledges the IUPAC glycopeptides project (AC-POL-09-11-25). A.H. is a SFI Stokes Senior Lecturer (07/SK/B1241). We thank Dr. Cormac O'Connell, Electron Microscopy Laboratory, University College Dublin, for access to TEM facilities.

Supporting information for this article is available on the WWW under <http://dx.doi.org/10.1002/anie.201208099>.

dispersibility, optimal  $T_1$ -weighting properties and selective binding.

The synthetic method (Scheme 1) involves the preparation of highly crystalline  $\text{Fe}_3\text{O}_4$  MNPs using the surfactant-free non-hydrolytic organic phase method.<sup>[8]</sup> The MNPs were further functionalized with 3-aminopropyl-triethoxysilane (APTS), which has been shown to be an effective initiator in the polymerization of amino acid *N*-carboxyanhydrides (NCA) from silica nanoparticles.<sup>[9]</sup> After APTS modification, thermogravimetric analysis (TGA) demonstrated the presence of ca. 15 mass% organic material (see the Supporting Information) and the MNPs were fully dispersible in nonpolar solvents, but not at all in water. The particle core diameter ( $d_{\text{core}}$ ) was calculated to be  $(8.3 \pm 2.0)$  nm, based on transition electron microscopy (TEM) images (Figure 1) with  $d_{\text{hyd}} = 12.9$  nm (PDI 0.14) in  $\text{CHCl}_3$ . The surface-amine-initiated ring-opening polymerization of propargyl-L-glutamate NCA<sup>[10]</sup> afforded polypeptide grafted MNPs (which were nondispersible in water) with clickable alkyne groups corresponding to a total organic mass of 38% (APTS plus polypeptide, based on TGA analysis; see the Supporting Information). The success of the grafting process in forming poly(propargyl-L-glutamate) (PPLG) on the surface was further verified by FTIR spectroscopy. The analysis showed

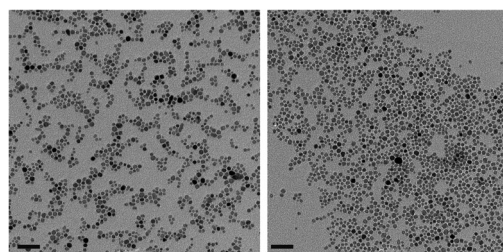


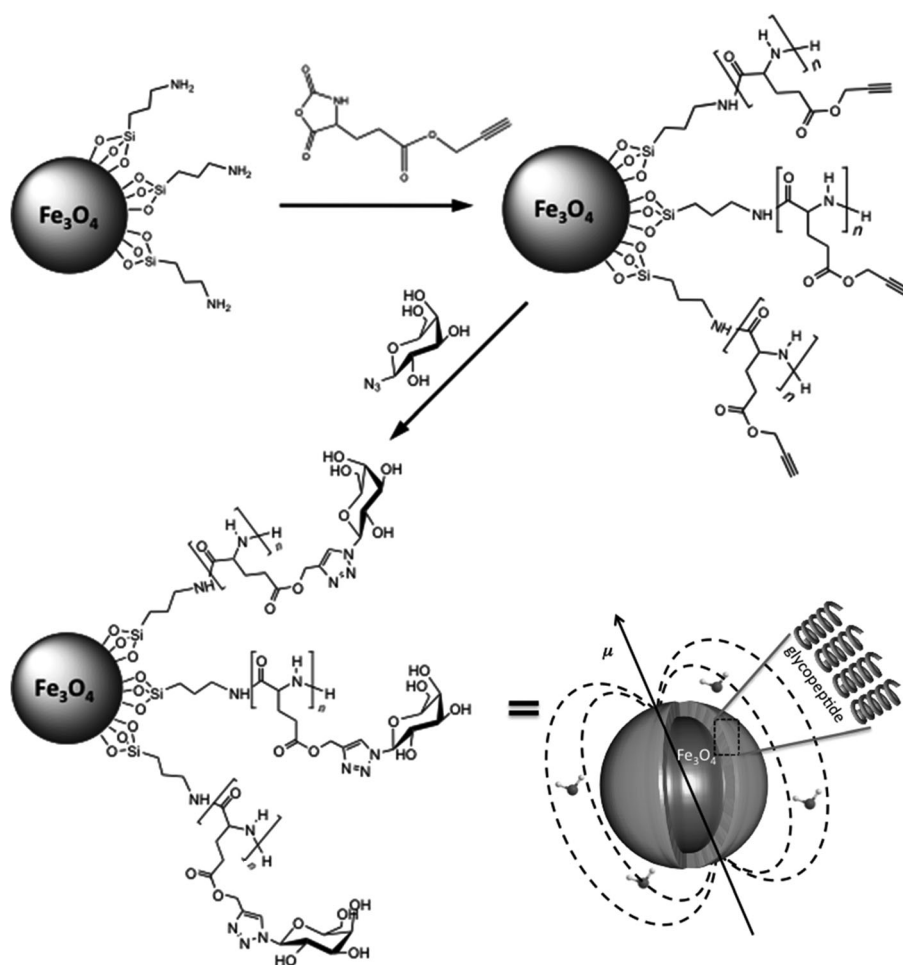
**Figure 1.** Representative transmission electron micrographs of APTS-functionalized  $\text{Fe}_3\text{O}_4$  NPs ( $d_{\text{TEM}} = (8.8 \pm 2.7)$  nm; left) and GP-MNPs ( $d_{\text{TEM}} = (8.3 \pm 2.0)$  nm; right). The scale bars are 50 nm.

distinct amide I and II bands at 1649 and  $1544\text{ cm}^{-1}$ , which are characteristic of an  $\alpha$ -helical conformation, and a glutamic ester carbonyl band at  $1725\text{ cm}^{-1}$ . Glycosylation was achieved by the Huisgen click reaction of azide-functionalized galactose to the surface bound PPLG. In agreement with the glycosylation FTIR spectra (see the Supporting Information), a strong galactose OH signal was observed at  $3296\text{ cm}^{-1}$ .<sup>[11]</sup> The glycosylation reaction was monitored by TGA analysis and, in a typical click reaction, an increase of ca. 18% in organic content upon glycosylation, relative to the PPLG functional MNP precursor particles, was measured. This

increase in mass corresponds to about 69% click efficiency. Energy-dispersive X-ray spectroscopy (EDAX) analysis before and after glycosylation also shows an increase in nitrogen content from 2.12 to 3.96%. Despite the poor resolution of the nitrogen peak, these values correspond to a click efficiency within 10% of the TGA value.

The resulting glycopeptide-grafted particles were easily dispersible in water, further highlighting the successful synthesis and extensive glycosylation. In water we find  $d_{\text{hyd}} = 15.5$  nm (PDI 0.12) by DLS, and this value did not change over a period of months (see the Supporting Information; stability in saline buffer and in serum has also been demonstrated). The low PDI value strongly suggests that the stable suspensions are composed of fully dispersed MNPs, which is critical for biological applications. This is consistent with the TEM analysis, which showed excellent quality MNPs with particle core diameters  $d_{\text{core}}$  of  $(8.3 \pm 2.0)$  nm (Figure 1).

The efficacy of GP-MNP dispersions for generating image contrast was studied primarily by fast field-cycling NMR relaxometry, or NMRD. The technique involves the measurement of  $r_1$  as a function of



**Scheme 1.** Synthesis of glycopeptide-grafted magnetic nanoparticles (GP-MNPs).

field strength (and hence  $^1\text{H}$  Larmor frequency). The profiles provide information on the particle size and magnetization, and more qualitative insights into the dynamics of the moment in its local magnetocrystalline field, using the  $^1\text{H}$  relaxation of water as a local probe. In this way NMRD can provide unique insights into magnetic order in suspensions of nanoparticles and their assemblies in situ.<sup>[12]</sup>

A typical NMRD profile of a GP-MNP dispersion is shown in Figure 2. The presence of a mid-frequency minimum is highly characteristic of superparamagnetic MNPs in suspension. The solid line included in Figure 2 is a simulation

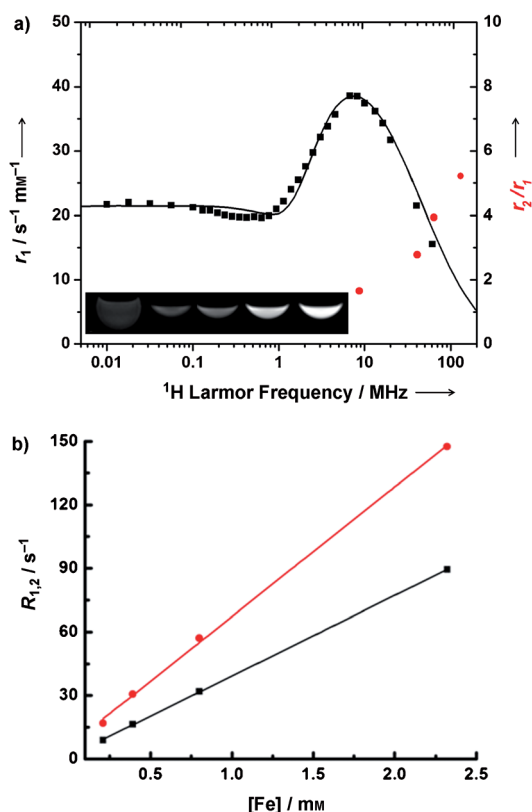


**Figure 2.** a)  $^1\text{H}$  relaxation profile (■) and relaxivity ratios (●), recorded at 298 K in  $\text{H}_2\text{O}$ , for a GP-MNP suspension,  $d_{\text{hyd}} = 15.5$  nm (PDI 0.12). The solid line is a simulation generated using SPM theory,<sup>[15]</sup> the parameters used were:  $d_{\text{core}} = 10$  nm,  $M_s = 59$  emu  $\text{g}^{-1}$ ,  $\Delta E_{\text{anis}} = 1.3$  GHz,  $\tau_N = 16$  ns (see text). The inset shows a  $T_1$ -weighted image recorded at 120 MHz. From the left: 0.0, 0.008, 0.04, 0.2, and 1.0 mm Fe. b) Determination of relaxivity,  $r_1$  (■) and  $r_2$  (●), at 9.25 MHz.

using SPM theory,<sup>[13]</sup> which is in very good agreement with the experimental data. The values obtained from this simulation are  $d_{\text{core}} = 10$  nm (slightly higher than TEM),  $M_s = 59$  emu  $\text{g}^{-1}$ ,  $\Delta E_{\text{anis}} = 1.6$  GHz, and  $\tau_N = 16$  ns. The low anisotropy energy and rapid Néel correlation time confirm the superparamagnetism, and hence dispersion, of the MNPs. SPM theory is known to produce slight overestimates in core size, but almost quantitative agreement with measured  $M_s$  values, for fully dispersed particles.<sup>[12a,14]</sup> The slight mid-frequency discrepancy arises because of a change in the relaxation mechanism in this range, which has been described.<sup>[15]</sup>

The utility of the GP-MNP dispersions for MRI is demonstrated by the values of the relaxivities,  $r_1$  and  $r_2$ . GP-MNPs have a high  $r_1$  of  $16 \text{ s}^{-1} \text{ mm}^{-1}$  and a low  $r_2$  of  $62 \text{ s}^{-1} \text{ mm}^{-1}$  at the typical clinical frequency of 61 MHz (1.5 T), which gives an  $r_2/r_1$  ratio of 3.9. In particular, the low ratio further demonstrates that the GP-MNPs are fully dispersed in water without any aggregation. The relaxivities confirm the applicability of the suspensions for  $T_1$ -weighted imaging at 60 MHz. Furthermore, the image (Figure 2, inset) demonstrates strong signal enhancement under  $T_1$ -weighting at 120 MHz. Hence, GP-MNPs may be useful over the human clinical MRI range. The relaxivities also shows that the polymer chains have minimal effect on the interaction of the magnetic moments with bulk water.

Most known MNP-based positive contrast agents are of slightly smaller size, and hence lower  $r_2/r_1$  ratio, but also have lower  $r_1$  values. Citrate-stabilized MNP dispersions of  $d_{\text{hyd}} = 7$  nm were considered as  $T_1$ -agents for MRI angiography,  $r_1 = 10.9 \text{ s}^{-1} \text{ mm}^{-1}$ ,  $r_2/r_1 = 2.4$ .<sup>[16]</sup> The medium-term stability in blood was an issue, this is presumably due to desorptive loss of citrate. PEGylated  $\text{Fe}_3\text{O}_4$  MNPs of the same core size, synthesized by ligand exchange of oleate, were also considered,<sup>[17]</sup> with similar results:  $r_1 = 7.3 \text{ s}^{-1} \text{ mm}^{-1}$ ,  $r_2/r_1 = 2.4$ . However, upon increasing the molecular weight of the polymer, as would be required for optimal steric stabilization and to achieve “stealth” effects in vivo, partial aggregation occurred, which compromised the  $T_1$ -weighting properties. By comparison, in our case the larger core used results in a favorable increase in  $r_1$ , which is partially offset by an increase in  $r_2/r_1$ ; however, the  $T_1$ -weighting potential remains. The grafting-from/click-functionalization strategy provides a robust and adaptable chemistry that ensures optimal colloidal properties (such as the prevention of particle aggregation, which is the key limitation for maintaining good  $T_1$ -weighting<sup>[17]</sup>), but also provides new potential for targeting. In this regard, it is important to emphasize that the surface chemistry we have described can be used for any APTS-coated iron oxide or metal ferrite MNP of any size.

To demonstrate specific targeting we used galactose functionalized GP-MNPs for binding to *Ricinus communis Agglutinin* ( $\text{RCA}_{120}$ ) lectin.<sup>[18]</sup> Figure 3 shows that, owing to the small size of the dispersed particles, a magnet has no effect on the GP-MNP dispersion in water (ca. 1.5 mm). The

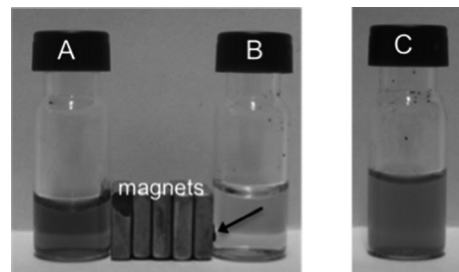


**Figure 3.** Dispersion of glycopeptide-grafted MNPs in water (1–2 mM) before (A) and after (B) the addition of lectin  $\text{RCA}_{120}$ . The addition of lectin causes particle aggregation (arrow) through selective multivalent binding and attraction to the magnet. C) Redispersion of MNPs through the addition of free galactose.



addition of RCA<sub>120</sub> causes particle aggregation through selective multivalent binding with the lectin, and attraction to the magnet. When additional galactose was added to the aggregated particles, competitive binding with free galactose resulted in the redispersion of MNPs. When the same experiment was carried out with Concanavalin A lectin (Con A), which is selective for glucosyl and mannosyl but unable to bind galactosyl residues, no aggregation was observed, thus highlighting the specific binding properties of the GP-MNPs.

There are no technical limits to the types, or indeed the combinations, of functional groups that can be used. This differentiates the current work from other approaches to fully disperse MNPs in water, which include stabilization with low- or intermediate-molecular-weight ligands. The most prominent of the former are citrate-stabilized dispersed MNPs, which have been assessed for clinical application;<sup>[16]</sup> however, desorption limited their colloidal stability and there was no potential for targeting. MNP stabilization with biologically derived ligands of intermediate molecular weight and lower charge (properties that reduce macrophage uptake) can be achieved by exchanging the alkyl ligands on MNPs, which have been synthesized by thermal decomposition, with bifunctional silanes<sup>[19]</sup> or phosphate-modified PEG.<sup>[18]</sup> However, yields can be low and the ligand density is often limited, in some cases compromising water stability. More recently, we reported a novel grafting-to approach using epoxy linker chemistry for binding amine-bearing polymers or amino acids, which yields fully dispersed MNP suspensions.<sup>[8b]</sup> Polymerization and MNP phase transfer (from THF to water) was achieved in a single step, which limited the possibility for targeting with active functional groups. Indeed, those limitations provided the motivation for the approach presented herein.

In summary, we have reported the first example of glycopeptide-stabilized hybrid MNPs, using NCA ring-opening polymerization to graft an alkyne-functionalized peptide from the particle surface followed by glycosylation through click chemistry. This approach produces biocompatible, monodisperse, highly crystalline superparamagnetic MNPs that are suitable for T<sub>1</sub>-weighted MRI. Furthermore, the click chemistry provides for any of a range of targeting (or optical) functional groups, with lectin specificity demonstrated here. The novel on-particle polymerization method is critical, as it generates a high surface density of anchoring points that can subsequently be functionalized as required. To our knowledge, this is the first example of highly dispersed particles where the density of functional groups is not limited by the NP surface area. In ongoing work we are extending our approach to assess the influence of the choice of sugar group(s) and polymer chain length on the MRI properties and the cellular uptake of MNPs. Our approach can be used to produce biologically compatible materials: the GP-MNPs are formed from iron oxide, amino acids, and monosaccharides, all of which are tolerated at clinical concentrations in humans. Finally, it should be noted that GP-MNPs could be used in responsive, or “smart” T<sub>2</sub>-weighted MRI; with signal sup-

pression following molecular recognition and subsequent controlled MNP aggregation.

Received: October 8, 2012

Published online: February 1, 2013

**Keywords:** click chemistry · glycopeptides · ligands · magnetic nanoparticles · ring-opening polymerization

- [1] a) M. E. Davis, Z. Chen, D. M. Shin, *Nat. Rev. Drug Discovery* **2008**, *7*, 771–782; b) R. A. Petros, J. M. DeSimone, *Nat. Rev. Drug Discovery* **2010**, *9*, 615–627.
- [2] J. Xie, G. Liu, H. S. Eden, H. Ai, X. Chen, *Acc. Chem. Res.* **2011**, *44*, 883–892.
- [3] K. El-Boubbou, D. C. Zhu, C. Vasileiou, B. Borhan, D. Prosperi, W. Li, X. Huang, *J. Am. Chem. Soc.* **2010**, *132*, 4490–4499.
- [4] L. Lartigue, C. Innocenti, T. Kalaivani, A. Awwad, M. Sanchez Duque, Y. Guari, J. Larionova, C. Guerin, J. G. Montero, V. Barragan-Montero, P. Arosio, A. Lascialfari, D. Gatteschi, C. Sangregorio, *J. Am. Chem. Soc.* **2011**, *133*, 10459–10472.
- [5] A. Pfaff, A. Schallon, T. M. Ruhland, A. P. Majewski, H. Schmalz, R. Freitag, A. H. E. Müller, *Biomacromolecules* **2011**, *12*, 3805–3811.
- [6] K. Babiuch, R. Wyrwa, K. Wagner, T. Seemann, S. Hoeppener, C. Remzi Becer, R. Linke, M. Gottschaldt, J. Weisser, M. Schnabelrauch, U. S. Schubert, *Biomacromolecules* **2011**, *12*, 681–691.
- [7] D. P. Gamblin, E. M. Scanlan, B. G. Davis, *Chem. Rev.* **2009**, *109*, 131–163.
- [8] a) N. Pinna, S. Grancharov, P. Beato, P. Bonville, M. Antonietti, M. Niederberger, *Chem. Mater.* **2005**, *17*, 3044–3049; b) T. Ninjbadgar, D. F. Brougham, *Adv. Funct. Mater.* **2011**, *21*, 4769–4775.
- [9] a) B. Fong, P. S. Russo, *Langmuir* **1999**, *15*, 4421–4426; b) T. Borase, M. Iacono, S. I. Ali, P. D. Thornton, A. Heise, *Polym. Chem.* **2012**, *3*, 1267–1275.
- [10] A. C. Engler, H. Lee, P. T. Hammond, *Angew. Chem.* **2009**, *121*, 9498–9502; *Angew. Chem. Int. Ed.* **2009**, *48*, 9334–9338.
- [11] a) J. Huang, G. Habraken, F. Audouin, A. Heise, *Macromolecules* **2010**, *43*, 6050–6057; b) J. Huang, C. Bonduelle, J. Thévenot, S. Lecommandou, A. Heise, *J. Am. Chem. Soc.* **2012**, *134*, 119–122.
- [12] a) E. Taboada, E. Rodriguez, A. Roig, J. Oro, A. Roch, R. N. Muller, *Langmuir* **2007**, *23*, 4583–4588; b) C. J. Meledandri, J. K. Stolarczyk, D. F. Brougham, *ACS Nano* **2011**, *5*, 1747–1755; c) C. J. Meledandri, D. F. Brougham, *Anal. Methods* **2012**, *4*, 331–341.
- [13] A. Roch, R. N. Muller, P. Gillis, *J. Chem. Phys.* **1999**, *110*, 5403–5411.
- [14] a) C. J. Meledandri, J. K. Stolarczyk, S. Ghosh, D. F. Brougham, *Langmuir* **2008**, *24*, 14159–14165; b) L. Xiao, J. Li, D. F. Brougham, E. K. Fox, N. Feliu, A. Bushmelev, A. Schmidt, N. Mertens, F. Kiessling, M. Valldor, B. Fadeel, S. Mathur, *ACS Nano* **2011**, *5*, 6315–6324.
- [15] S. Laurent, D. Forge, M. Port, A. Roch, C. Robic, L. Vander Elst, R. N. Muller, *Chem. Rev.* **2008**, *108*, 2064–2110.
- [16] M. Taupitz, S. Wagner, J. Schnorr, I. Kravec, H. Pilgrimm, H. Bergmann-Fritsch, B. Hamm, *Invest. Radiol.* **2004**, *39*, 394–405.
- [17] U. I. Tromsdorf, O. T. Bruns, S. C. Salmen, U. Beisiegel, H. Weller, *Nano Lett.* **2009**, *9*, 4434–4440.
- [18] S. G. Spain, N. R. Cameron, *Polym. Chem.* **2011**, *2*, 1552–1560.
- [19] R. De Palma, S. Peeters, M. J. Van Bael, H. Van den Rul, K. Bonroy, W. Laureyn, J. Mullens, G. Borghs, G. Maes, *Chem. Mater.* **2007**, *19*, 1821–1831.